Journal of Hydrology 601 (2021) 126677

Contents lists available at ScienceDirect

Journal of Hydrology

journal homepage: www.elsevier.com/locate/jhydrol

Research papers

Characterization of a multi-layer karst aquifer through analysis of tidal fluctuation

Hua Zhang

Southwest Florida Water Management District (SWFWMD), 2379 Broad Street, Brooksville, FL 34604, USA

ARTICLE INFO

This manuscript was handled by Corrado Corradini, Editor-in-Chief, with the assistance of Yongjun Jiang, Associate Editor

Keywords:
Karst aquifer
Jacob-Ferris equation
Tidal fluctuations
Coastal springs

ABSTRACT

Interaction between ocean tides and coastal aquifers is an important process influencing the quality and quantity of groundwater resources. In this study, high frequency groundwater fluctuation along two transects from the Gulf of Mexico to the Upper Floridan Aquifer (UFA) were analyzed to characterize the hydrogeologic structure of the multi-layer karst aquifer. Tidal efficiency and time lag of harmonic constants were calculated from groundwater and seawater level and aquifer diffusivity were estimated using the Jacob-Ferris equation. Measurable tidal signals were observed at a maximum inland distance of approximately 7–8 km due to the high conductivity of the unconfined karst aquifer. The largest tidal fluctuation was observed in the deeper unit of the aquifer (146–155 m below land surface), which indicate the hydraulic contact between seawater and the high permeability zone of Avon Park Formation. The estimated values of hydraulic diffusivities agreed well with the regional groundwater flow model despite the highly heterogeneous nature of karst aquifer. Our analysis suggested that tidal springs are important sea water/groundwater interfaces and the conduit networks of tidal creeks, caves, and fractures are preferential pathways of tidal propagation.

1. Introduction

Tidal fluctuation is a ubiquitous force that constantly impacts the high-frequency variation of coastal groundwater levels (Jiao and Post, 2019). Extensive studies have been dedicated to understanding mechanisms of tidal propagation in coastal aquifers. Research revealed that tidal amplitude exponentially decreased and phase increasingly shifted as the tidal wave traveled landward. The degree of amplitude damping and phase shift is controlled by 1) tidal amplitude and frequency; 2) location, geometry, and slope of the aquifer/seawater interface; 3) aquifer character (confined, unconfined, or leaky); and 4) hydraulic properties (storativity/specific yield, hydraulic conductivity, and aquifer thickness).

An analytical solution of one-dimensional flow in homogeneous and infinite aquifer subject to periodic head oscillation at an ocean boundary was derived by Jacob (1950) and Ferris (1951) and has been extensively employed to estimate hydraulic properties (e.g., Nielsen, 1990; Trefry and Johnston, 1998; Merritt, 2004; Rotzoll et al., 2008, 2013; Trglavcnik et al., 2018). Later on, numerous analytical solutions were derived for special cases, e.g., aquifer extended beneath sea floor (van der Kamp, 1972), aquifer near tidal rivers (Maas and de Lange, 1987), sloping beaches (Nielsen, 1990; Cartwright et al., 2004), layered aquifer with a unconfined and confined aquifer separated by a thin aquitard (Jiao and Tang, 1999), leaky aquifer (Li and Jiao, 2001; Xia et al., 2007), dual-tide propagation around the island (Trefry and Bekele, 2004; Sun et al., 2008; Rotzoll et al., 2008), capillary rise in vadose zone (Kong et al., 2015), multi-layer aquifers (Guo et al., 2007; Bakker, 2019), and randomly distributed conductivity fields (Trefry et al., 2011). The analytical solutions assume a homogeneous aquifer with uniform storativity and conductivity, which may result in high degree of uncertainty when applied to highly heterogenous aquifers. Numerical models have been employed to investigate the groundwater head and flow response to period forcing in heterogeneous geologic media (Ataie-Ashtiani et al., 2001; Riedel et al., 2010). Furthermore, studies have been conducted using density-dependent flow models to investigate the impact of tidal forcing on salt water intrusion (Mao et al., 2006; Li et al., 2008; Post, 2011; Mulligan et al., 2011; Kuan et al., 2012; Abarca et al., 2013; Pauw et al., 2014; Xin et al., 2015). Inverse modeling has been conducted to estimate hydraulic parameters from observed tidal response in groundwater (Alcolea et al., 2007; Jardani et al., 2012).

In general, tidal signals propagate farther in the confined aquifer than in the unconfined aquifer. The rapid damping of tidal pressure waves in unconfined aquifers is believed to be a result of its specific yield, which is usually several orders of magnitude higher than

E-mail address: hua.zhang@swfwmd.state.fl.us.

https://doi.org/10.1016/j.jhydrol.2021.126677
Received 6 May 2021; Received in revised form 7 July 2021; Accepted 9 July 2021
Available online 15 July 2021

storativity of confined aquifers. Nielsen (1990) reported that tidal amplitude quickly reduced from 0.516 m on the shore to 0.075 m as it traveled to about 25 m from the shore. Field observation of Erskine (1991) reported that tidal oscillations were unmeasurable 400 m from the shore. However, for unconfined aquifers with exceptionally high transmissivities, the tidal effects may be observed much further inland. For example, the monitoring well at the center of an island aquifer, about 5 km to shore, showed clear major tidal modes (Rotzoll et al., 2008). Furthermore, tidal fluctuation in unconfined aquifers can vary substantially with depth in multi-unit aquifers, whereas field studies showed larger amplitude and smaller time lags in deeper units (Erskine, 1991; Trefry and Johnston, 1998). Nevertheless, tidal fluctuation in multi-unit unconfined karst aquifers were scarcely studied and little is known regarding the role of conduit network in tidal propagation (Martin et al., 2012; Perriquet et al., 2014).

The objectives of this study are: 1) to determine the vertical and horizontal extent of tidal propagation in a multi-unit unconfined karst aquifer through analysis of continuous groundwater monitoring records; and 2) to evaluate the feasibility and limitations of analytical equations for calculating the hydraulic parameter of highly heterogenous karst aquifers. It is also expected the study can shed light on the potential role of fracture network in transmission of tidal fluctuation in aquifers.

2. Material and methods

2.1. Study site

The study site is located on the west coast of the Florida Peninsula and eastern side of the Gulf of Mexico (Fig. 1). The study area lies within the physiographic regions of Coastal Swamps and Gulf Coastal Lowlands, which has a typical karst landscape with numerous springs, sinkholes, internal drainage, and undulating topography. The land altitudes gradually increase from sea level at the gulf coast to about 15 m above sea level along the eastern edge of the study area. The long-term mean annual rainfall is about 1,372 mm and ranged from 1,016 to 1,803 mm. Monthly rainfall is concentrated in June through September and heavily impacted by convective thunderstorms during summer and tropical storms during hurricane season.

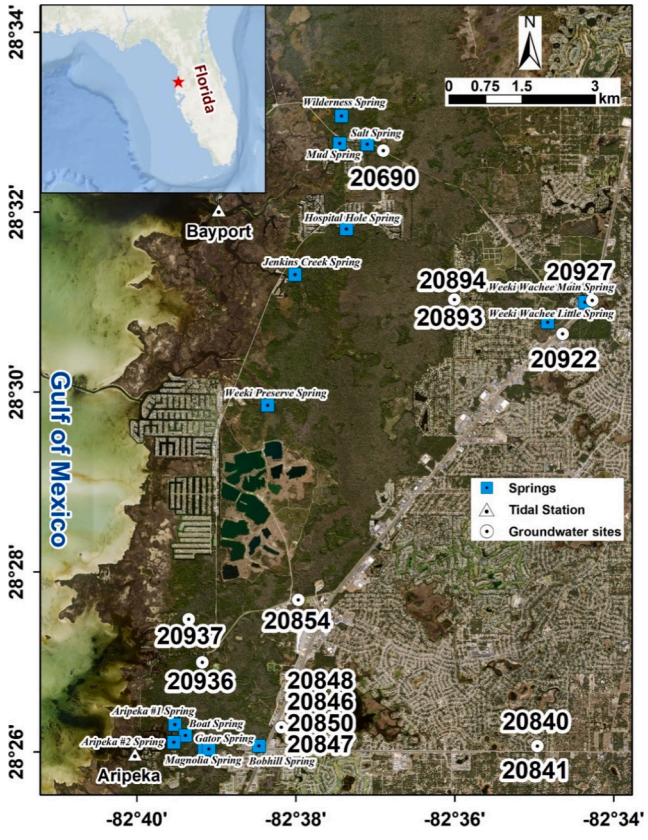

Fig. 1. Location map and aerial image displaying the sites of groundwater monitoring wells, tidal stations, and springs. The altitudes increase from sea level at the gulf coast to about 15 m above Mean Sea Level on the east boundary.

The coastal springs and estuaries of west-central Florida provide a unique and important ecological setting for submerged aquatic vegetation, benthos, mollusks, fish, and manatees. Ecological integrity in spring-fed estuaries is directly connected to salinity, which is controlled by the quantity and quality of water discharging from the springs. Seasonal pattern of spring flow is generally proportional to the groundwater level in coastal aquifers and is affected primarily by rainfall induced recharge. Many of the springs are characterized as tidal controlled with discharge greatly affected by sea level variation (Yobbi, 1992; Knochenmus and Yobbi, 2001; Chen, 2012; Menning et al., 2015).

2.2. Hydrogeology

The hydrological system is part of the coastal springs groundwater basin bounded by groundwater divides rather than topographic divides, where the principal drainage is groundwater flow through springs and creeks and there is minimal surface drainage (Yobbi, 1992). The Weeki Wachee Springs groundwater basin in the north contains the Weeki Wachee Main Spring and numerous smaller springs including Little, Wilderness, Salt, Mud, Hospital Hole, and Jenkins Springs (Fig. 1). The Weeki Wachee Main and Little Springs discharge freshwater and available data shows that spring flows are not influenced by tide. Salt, Mud, and Jenkins Springs discharge brackish water and are tidally influenced. The springs discharge to the Weeki Wachee River, which meanders about 11.9 km to the Gulf of Mexico at Bayport in Hernando County, Florida. Most of the flow in the river is from Weeki Wachee Main Spring, with average discharge of approximately 4.93 m^3/s for the period of record (Knochenmus and Yobbi, 2001). The Aripeka Springs groundwater basin in the south contains many small springs including Aripeka #1, Aripeka #2, Boat, Gator, Magnolia, and Bobhill Springs, which are clustered in a 2.5 km^2 area (Fig. 1). Flow of the springs are tidally affected and discharge a mixture of saltwater and freshwater. The spring discharge were collected by the Hammock Creek and then flows about 1.6 km to the Gulf of Mexico. Flow in Hammock Creek is tidally controlled (Knochenmus and Yobbi, 2001; Menning et al., 2015).

The groundwater flow is part of the Floridan aquifer system, which is one of the most productive aquifer systems in the Unites States and the primary water source for the rapidly increasing population and economy in the region. It is predominantly carbonate sequence of the Paleocene to Lower Miocene Series (Ryder, 1985; Williams and Kuniansky, 2016). In the study area, the hydrogeologic framework includes a discontinuous surficial aquifer (SA) system consisting of unconsolidated deposits of sand and clay, and a thick carbonate Upper Floridan Aquifer (UFA) exposed at or very near to the land surface (Fig. 2). The UFA is largely unconfined and experiences rapid recharge and increased discharge following rainfall events (Yobbi, 1992; Knochenmus and Yobbi, 2001).

The geologic units of UFA include the Suwannee Limestone of Oligocene age, the Ocala Limestone and the Avon Park Formation of Eocene age (Fig. 2). Field tests indicate that the Suwannee Limestone and Ocala Limestone have moderate to high porosity and permeability. The more consolidated limestone near top of the Avon Park Formation results in a low permeability zone, under which is a high permeability zone (start from about 125 m below land surface) with extensive cavities, fractures, and other solution features. The high permeability zone of the Avon Park Formation is the deepest unit containing freshwater water and its bottom (approximately 240 m below land surface) coincides with the bottom of the UFA, which is characterized by the persistent occurrence of evaporites (Yobbi, 1992; Knochenmus and

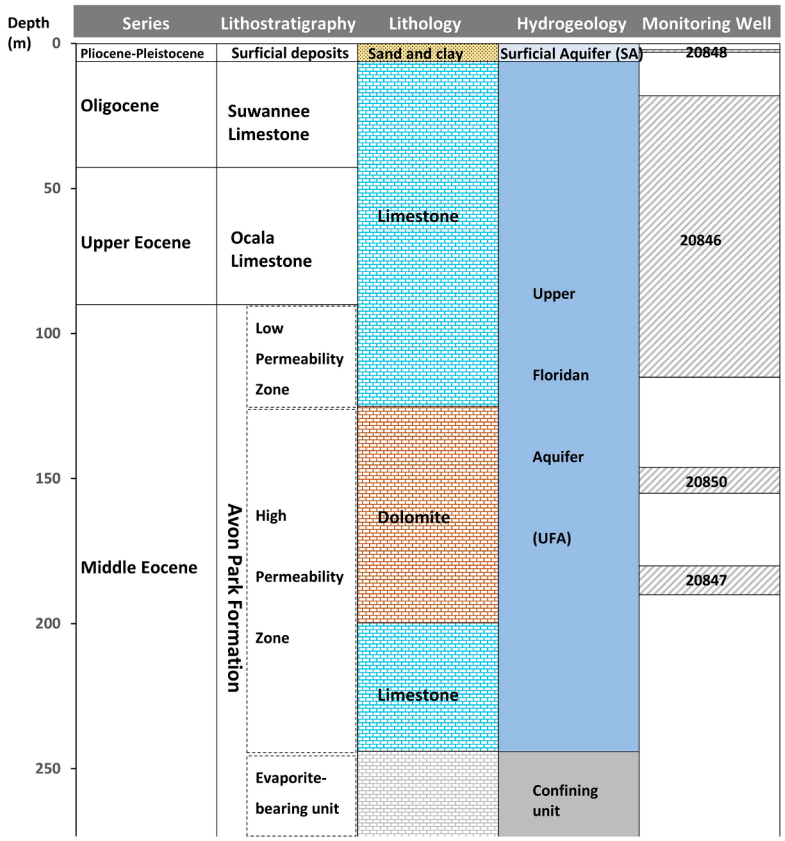

Fig. 2. Generalized correlation chart for stratigraphic and hydrogeologic units at the monitoring site ROMP TR18-3 with the sampling depth of the 4 monitoring wells (20848, 20846, 20850, and 20847).

Yobbi, 2001).

The groundwater in UFA generally flows west to northwest from the high potential zone inland and discharges to the Gulf of Mexico as diffuse seepage along the coast or through springs. Recharge occurs as rapid infiltration through surficial deposits and drainage into sinkholes, followed by fast flow through secondary porosity features such as conduits, enhanced fracture zones, or caverns within the limestone. The discharge occurs in the form of upward flows through solution cavities to springs or diffusive upward leakage into coastal swamps or the near-shore environment. The freshwater-saltwater transition zone has a diffusive interface parallel to the coast with landward reentrants at major springs (Yobbi, 1992; Menning et al., 2015).

2.3. Data source

Sea water level data recorded at the Aripeka Coastal Station (ARPF1) was downloaded from National Data Buoy Center (NDBC) of National Oceanic and Atmospheric Administration (NOAA) (https://www.ndbc.noaa.gov/station_page.php?station=arpf1). Station ARPF1 (Fig. 1) is a shore-based tower station mounted on the South Fork Hammock Creek Bridge. It is operated by the Coastal Ocean Monitoring and Prediction System (COMPS) of the University of South Florida (USF). Measured sea level time series at 6-minute intervals in the year 2019 were used in the tidal harmonic analysis. Sea level data at the Bayport coastal station (USGS 02310600) was obtained from the National Water Information System (NWIS) (https://waterdata.usgs.gov/nwis) of United Sates Geological Survey (USGS). Measured sea level time series at 15-minute intervals in the year 2019 were used in the tidal harmonic analysis. A one-week subset of measured sea level variation at the tidal stations is illustrated in Fig. 3.

The groundwater data in this study was measured in Regional Observation and Monitor-Well Program (ROMP) well sites, which were constructed and operated to monitor the freshwater-saltwater interface by the Southwest Florida Water Management District (SWFWMD). Hourly water level measurements have been continuously recorded with submersible pressure transducers at an operating precision of ± 1.5 mm since 1997. Time series data of year 2019 were retrieved and used in this study. Location of the well sites are shown in Fig. 1 and the physical settings such as land surface elevation, casing and total depth are given in Table 1. The natural coast of this area is characterized by tidal flats extending many kilometers into the Gulf and a lack of clear shoreline. For our analysis, the nearest tidal pool was identified on the high-resolution aerial image of 2009 and the distances to the nearest tidal pool were measured for each monitoring well.

2.4. Water level analysis

Water levels measured at the tidal station and monitoring wells were all converted to North American Vertical Datum of 1988 (NAVD 88). The measured time series of groundwater levels were detrended to eliminate low frequency fluctuations caused by natural and anthropogenic stresses such as rainfall-evaporation, groundwater withdrawal, and aperiodic atmospheric pressure variations. Specifically, 24-hour moving averages were subtracted from observed hourly time series to detect the diurnal/semi-diurnal tidal variations (Merritt, 2004). An example of fortnight variation of measured and detrended groundwater level is illustrated in Fig. 4 for monitoring well 20850 (ROMP TR18-3 Avon Park Formation). The detrended values of groundwater levels were used for the tidal harmonic analysis and hydraulic parameter estimation.

Monitoring data along 2 transects from the Gulf of Mexico to inland were analyzed to quantify the impact of tidal dynamics on groundwater level of SA and UFA (Fig. 1). Groundwater level of the 5 monitoring wells (1 SA well and 4 UFA wells) along the Weeki Wachee transect were

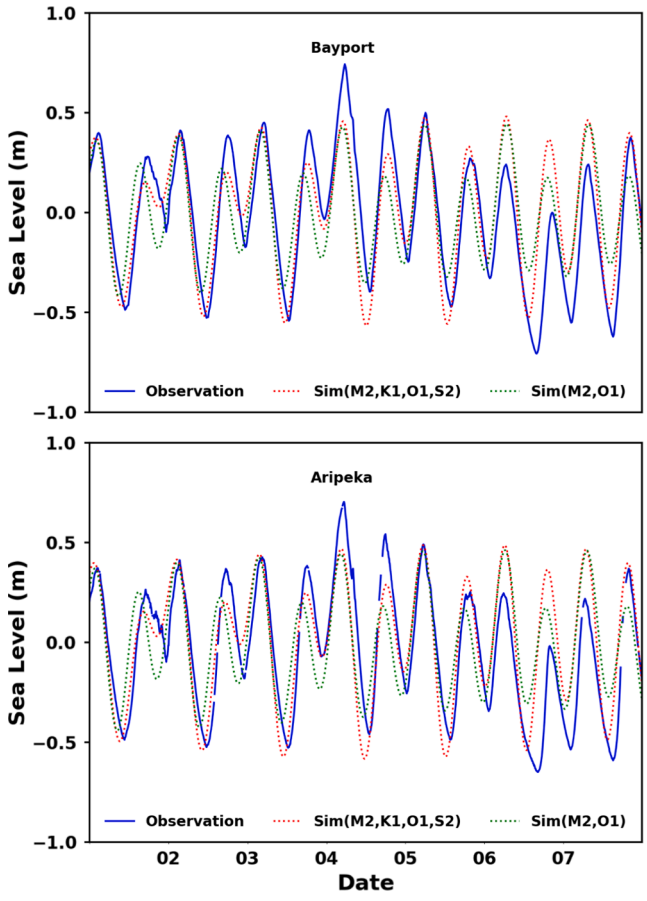

Fig. 3. Measured and simulated sea water level at Bayport (USGS 02310600) and Aripeka (NOAA ARPF1) coastal stations from 2019/03/01 to 2019/03/07. Solid blue lines are measured sea level (NAVD 88). The red dotted lines are simulated sea level using harmonic constants of four tidal components (M2, K1, O1, S2) given in Table 3 and the green dotted lines are simulated with harmonic constants of M2 and O1 given in Table 4. (For interpretation of the references to colour in this figure legend, the reader is referred to the web version of this article.)

compared with the sea level variation at Bayport coastal station (USGS 02310600). Similarly, the Aripeka transect in the south has 9 monitoring wells (2 SA wells and 7 UFA wells) and the measured groundwater levels were compared with sea level of the Aripeka Coastal Station (ARPF1). There are 4 wells (20848, 20846, 20850, and 20847) opening to different geologic units at site ROMP 18-3 on the Aripeka Transect, which was used to characterize the vertical distribution of tidal variations in the multi-unit aquifers. One-week subsets of detrended groundwater level comparison with the measured tidal elevations are illustrated for selected wells in Figs. 5 and 6.

Cross correlations were performed to determine the time-lagged interrelation of measured sea level with detrended groundwater levels (Schaff and Richards, 2014). The Pearson correlation coefficient (r) were computed between time series pairs in 1-minutes time windows. The time shift corresponding to the maximum r (r_{lag}) were determined as the time lag (t_{lag}) between the groundwater level and sea level. Linear regression was carried out between shifted groundwater level and sea level and the slope of regression was computed as the relative amplitude (A_R). Here we assume that the diurnal fluctuation of groundwater (h_{gl}) is a linearly scaled signal of the corresponding sea level fluctuation (h_{sl}) that can be expressed as $h_{gl} = A_R h_{sl} + n$, where n is uncorrelated noise.

2.5. Tidal harmonic analysis

Tidal harmonic constants were estimated by least square fitting of measured sea levels or detrended groundwater levels to the function:

$$h(t) = h_0 + \sum \alpha_i \cos(\omega_i t + \phi_i) \quad (1)$$

where h is the tidal variation around mean sea level (h_0), t is time, α_i is the amplitude of tidal constituent i, ω_i and ϕ_i are the angular frequency and phase constants, respectively. The angular frequencies of tidal constituents $\omega_i = \frac{2\pi}{\tau_i}$, where τ_i are the periods of tidal constituents M2 (12.42 h), O1 (25.82 h), K1 (23.93 h), S2 (12 h).

The analysis was carried out using UTide code (Codiga, 2011). In the initial analysis, α_i and ϕ_i of 4 major tidal constituents (M2, S2, O1, and K1) were estimated at each tidal station or groundwater well. The solar component (K1 and S2) may contain atmospheric-pressure and is considered unsuitable for estimation of hydraulic parameters (Merritt, 2004). Therefore, a second analysis was conducted where the time series were fitted with only two tidal constituents (M2 and O1) to obtain α_i and ϕ_i. The tidal variations at different sites were simulated using the computed harmonic constants. Example of simulated tidal fluctuations are illustrated in Fig. 3 for tidal stations and Fig. 4 for groundwater well.

Tidal efficiency factor (T_e) is defined as the tidal amplitude of the groundwater level (α_{gl}) divided by that of the seawater level (α_{sl}):

$$T_e = \frac{\alpha_{gl}}{\alpha_{sl}} \quad (2)$$

In addition, the phase lag ($\Delta\phi$) of each groundwater well is calculated as the difference between phase constants of groundwater level (ϕ_{gl}) and seawater level (ϕ_{sl}):

$$\Delta\phi = \phi_{gl} - \phi_{sl} \quad (3)$$

2.6. Calculation of aquifer diffusivity

Under the assumption of homogenous and isotropic aquifer with only horizontal flow, the groundwater flow can be described with the 1D linear groundwater flow equation:

$$\frac{\partial h}{\partial t} = D\frac{\partial^2 h}{\partial x^2} \quad (4)$$

where h is the groundwater level, x is the horizontal distance from observation wells to the nearest tidal pool. $D = \frac{T}{S}$ is the aquifer diffusivity, where T is the transmissivity and S is the storativity. The governing equation subject to tidal boundary condition in Eq. (1) at the ocean side ($x = 0$) and a constant groundwater level at the inland side:

$$h(0,t) = h_0 + \sum \alpha_i cos(\omega_i t + \phi_i) \quad (5a)$$

$$h(\infty, t) = h0 \quad (5b)$$

Eq. (4) subject to boundary conditions specified in Eq. (5) was analytically solved (Jacob, 1950; Ferris, 1951):

$$h(x,t) = h_0 + \alpha_i e^{-x\sqrt{\frac{\omega_i}{2D}}} cos\left(\omega_i t + \phi_i - x\sqrt{\frac{\omega_i}{2D}}\right) \quad (6)$$

Eq. (6) is commonly referenced as the Jacob-Ferris equation, which predicts that the tidal efficiency (T_e) exponentially decays with inland distance:

$$T_e(x) = e^{-x\sqrt{\frac{\omega_i}{2D}}} \quad (7)$$

and the phase lag ($\Delta\phi$) linearly increases with inland distance:

$$\Delta\phi(x) = -x\sqrt{\frac{\omega_i}{2D}} \quad (8)$$

Table 1
Summary description of groundwater monitoring wells in this study.

Site ID	USGS ID	Site	Hydrogeology	Surface Elevation[a](m)	Casing Depth(m)	Total Depth(m)	Water Table[b](m)	Distance to shore[c](km)	Distance to tidal pool[c](km)
Weeki Wachee Transect									
20690	283243082365701	ROMP TR19-2	Avon Park Formation	2.7	84	92	1.52	2.9	0.83
20894		WW-4 Weeki Wachee	Surficial deposits	5.1	2.1	8.2	2.72	4.8	3.7
20893	283101082360401	WW-4 Weeki Wachee	Avon Park Formation	5.1	147	159	2.43	4.8	3.7
20927	283104082341801	Weeki Wachee Springs	Ocala Limestone	7.2	37	80	3.56	7.6	5.7
20922	283043082344101	Weeki Wachee	Ocala Limestone	14.0	19	93	3.47	7.2	5.9
Aripeka Transect									
20937	282750082391001	ROMP TR18-2A	Ocala Limestone	1.8	47	64	1.12	1.5	0.5
20936	282659082391104	ROMP TR18-2	Avon Park Formation	2.0	136	146	2.60	1.4	0.9
20848	282613082381703	ROMP TR18-3	Surficial deposits	6.4	2.1	3.0	4.20	3.1	2.2
20846	282613082381701	ROMP TR18-3	Ocala Limestone	6.4	18	115	4.10	3.1	2.2
20850	282613082381702	ROMP TR18-3	Avon Park Formation	6.4	146	155	4.06	3.1	2.2
20847	282613082381704	ROMP TR18-3	Avon Park Formation	6.4	180	190	4.02	3.1	2.2
20854	282742082375901	ROMP TR18-1	Avon Park Formation	4.7	136	177	4.30	3.7	2.7
20840		ROMP 97	Surficial deposits	10.0	1.8	7.9	6.22	8.3	7.3
20841	282605082345801	ROMP 97	Avon Park Formation	11.0	94	108	6.18	8.3	7.3

[a] Elevation above Mean Sea Level, NAVD 88.
[b] *Water Table*: Mean groundwater level measured in year 2019, NAVD88.
[c] Distance to the nearest tidal pool measured on aerial image.

Eqs. (7) and (8) provide two ways of estimating aquifer diffusivity:

$$D_\alpha = \left[\frac{x}{\ln(T_e)}\right]^2 \frac{\omega_i}{2} \tag{9}$$

$$D_\phi = \left[\frac{x}{\Delta\phi}\right]^2 \frac{\omega_i}{2} \tag{10}$$

where D_α and D_ϕ are hydraulic diffusivity estimated from tidal efficiency or phase lag, respectively (Merritt, 2004). To apply the equations, linear regression was conducted to calculate slopes (b_α) of $\ln(T_e)$ versus distance to shore (x) and then D_α is calculated as

$$D_\alpha = \frac{\omega_i}{2{b_\alpha}^2} \tag{11}$$

Similarly, slope (b_ϕ) is calculated from linear regression between phase lag ($\Delta\phi$) and distance (x). Then D_ϕ is calculated as

$$D_\phi = \frac{\omega_i}{2{b_\phi}^2} \tag{12}$$

where b_ϕ is the slope of linear regression between $\Delta\phi$ and x.

3. Results

3.1. Landward tidal dissipation

One year of measured groundwater levels for 3 Floridan Aquifer wells (20690, 20893, 20922) on the Weeki Wachee transect are shown in Fig. 7a together with time series of tidal elevation at the Bayport coastal station. Fortnight subsets of detrended groundwater levels are illustrated in Fig. 7b to compare the tidal amplitudes with sea level. The tidal elevation at Bayport station exhibited a clear semi-diurnal pattern with diurnal fluctuation over 1.0 m (Fig. 3a). The monitoring well near the coast (20690, 0.9 km inland and 0.83 km from the nearest tidal pool) exhibited the largest fluctuation in response to the tidal wave, with a diurnal fluctuation around 0.4–0.6 m (Figs. 5a and 7b). The patterns of groundwater level at wells further inland (20893 and 20922) mostly exhibited seasonal variation controlled by the regional weather patterns. The monitoring well 20893 (4.8 km inland and 3.7 km from tidal pool) exhibited a damped diurnal variation about 0.10–0.15 m (Fig. 5b and 7b). The tidal signal is severely damped but still detectable at the most inland well 20922 (7.2 km inland and 5.9 km from tidal pool), with an amplitude around 0.010–0.015 m (Fig. 5c and 7b). Detailed comparison of groundwater diurnal variation with sea level in Fig. 5 indicated increased phase shift as tidal waves propagated landward.

A time series regression with lagged variables was carried out to establish the cross correlation between groundwater and seawater levels. The calculated time lagged correlation coefficients (r_{lag}), relative amplitude (A_R) and time lag (t_{lag}) are given in Table 2. Strong correlation between the Floridan Aquifer water level and tidal variation are revealed by the high values of correlation coefficients. Groundwater well 20922 ($r_{lag} = 0.587$) and 20927 ($r_{lag} = 0.613$) with inland distances > 5 km had significant correlation with the sea level at the Bayport station. The cross-correlation analysis also exposed the fast propagation of tidal signals in this unconfined Karst aquifer, as shown by the values of time lag (t_{lag}). The results suggest that it takes 1.6 h for the tidal wave to reach 5.7 km inland at site 20927 and the tidal amplitude at site 20927 is 0.74% of the ocean tide.

Similarly, measured groundwater levels for 4 Floridan Aquifer wells (20936, 20850, 20854, 20841) on the Aripeka transect displayed a landward attenuation of tidal fluctuation (Fig. 8). However, the tidal propagation along the Aripeka transect is relatively slower and weaker than along the Weeki Wachee Transect. The tidal elevation at coastal station Aripeka is close to that of the Bayport station with similar amplitude and slight shift (Fig. 3). At well 20936 (1.4 km inland and 0.9 km to tidal pool), $A_R = 0.094$ and $t_{lag} = 0.92$ h (Fig. 6a and Table 2). A weak tidal signal was detected at 8.3 km inland (site 20841 with$r_{lag} = 0.273$ and$A_R = 0.0031$) and time lag is 2.92 h . At site 20854 (3.7 km inland and 2.2 km to tidal pool), the tidal signal is 3.55 h behind the tidal station, indicating the relatively slow propagation of tidal wave to this

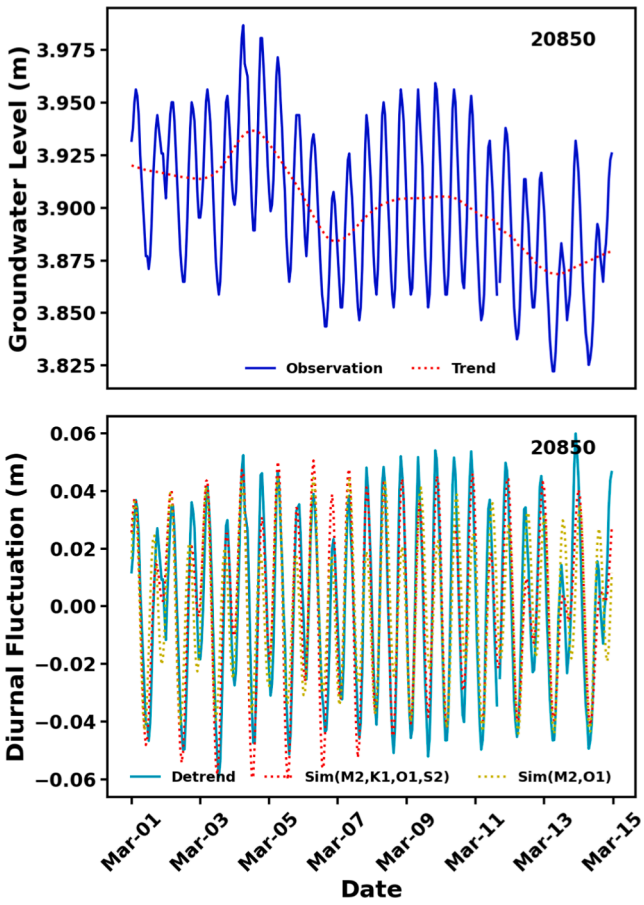

Fig. 4. Measured and simulated groundwater level at monitoring well 20850 (ROMP TR18-3 Avon Park Formation) from 2019/03/01 to 2019/03/14. top) Measured groundwater level (solid blue line) and low frequency trend calculated as 24-hour moving average (dashed red line); b) Detrended groundwater level (solid cyan line) and simulated tidal fluctuation. The red dotted lines are simulated groundwater level using harmonic constants of four tidal components (M2, K1, O1, S2) given in Table 3 and the green dotted lines are simulated with harmonic constants of M2 and O1 given in Table 4. (For interpretation of the references to colour in this figure legend, the reader is referred to the web version of this article.)

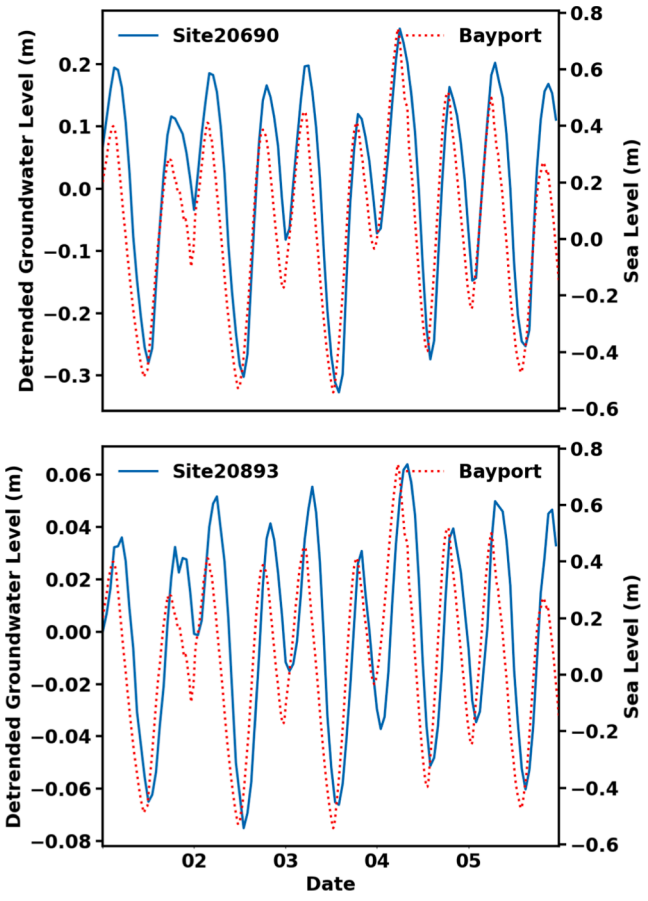

Fig. 5. Comparison between measured sea level and detrended groundwater level from 2019/03/01 to 2019/03/05. top) Bayport tidal station vs. site 20690 (ROMP TR19-2 Ocala Limestone); bottom) Bayport tidal station vs. site 20893 (WW4 Avon Park Formation).

site away from spring consuits.

3.2. Tidal propagation in multi-layer aquifer

The diurnal fluctuation of groundwater level in all 3 surficial aquifer wells (20894, 20848, 20840) were below or near the detection limit. The cross-correlation analysis result in Table 2 showed that there is a weak correlation between the groundwater level in well 20894 on the Weeki Wachee transect (4.8 km to shore and 2.1 m depth) with sea level (r_{lag} = 0.13 andA_R = 0.0044). No significant correlation between groundwater and sea level were detected for the two surficial wells 20848 and 20840 on the Aripeka transect. The result indicated that tidal variation was very weak or undetectable in surficial aquifer wells regardless of their distance to shore.

One year of measured groundwater levels for 4 wells (20848, 20846, 20850, 20847) open to different hydrogeologic layers at the site ROMP 18-3 (3.1 km inland and 2.2 km to tidal pool) are illustrated in Fig. 9a and fortnight subsets of detrended groundwater levels are depicted in Fig. 9b. The 4 wells at different layers exhibited similar seasonal patterns in response to the recharge and evapotranspiration conditions (Fig. 9a). The groundwater elevation of surficial aquifer well 20848 (casing depth of 2.1 m) is slightly higher than the 3 Upper Floridan Aquifer wells.

The 3 Floridan aquifer monitoring wells (20846, 20850, 20847) at ROMP 18–3 (2.2 km inland) demonstrated vertical pattern of tidal fluctuation in the Floridan Aquifer (Fig. 9b). It is found that the well 20850 (casing depth of 146 m and total depth of 155 m) open to high permeable zone of the Avon Park Formation has the strongest correlation with tidal signal (r_{lag} = 0.888), with highest relative amplitude A_R = 0.080 and smallest time lag t_{lag} = 0.78 h at ROMP 18–3 (Fig. 6b and Table 2). The groundwater well 20846 (casing depth of 18 m and total depth of 115 m) open to the Ocala Limestone had a much smaller tidal amplitude (A_R = 0.046) than that of the Avon Park Formation. The result indicated the tidal signal is preferentially propagated through the high permeable zone of the Avon Park Formation. Comparison between the well 20937 (casing depth of 47 m and total depth of 64 m) and 20936 (casing depth of 136 m and total depth of 146 m) exhibited a similar pattern with the stronger tidal fluctuation in the Avon Park Formation than the Ocala Limestone (Table 2). Unfortunately, there is no comparable well pairs between the Avon Park Formation than the Ocala Limestone on the Weeki Wachee transect. But the relative amplitude values in Table 2 revealed that the 2 wells open to the Avon Park Formation (20690 and 20893) had much larger tidal fluctuations than the 2 wells open to the Ocala Limestone (20922 and 20927).

3.3. Tidal amplitude and phase

The amplitude (α_i) and phase shift (ϕ_i) of each tidal component were estimated from fitting the seawater level or detrended groundwater levels using the least-square curve fitting method and the computed parameter values are given in Tables 3 and 4 with the 95% confidence

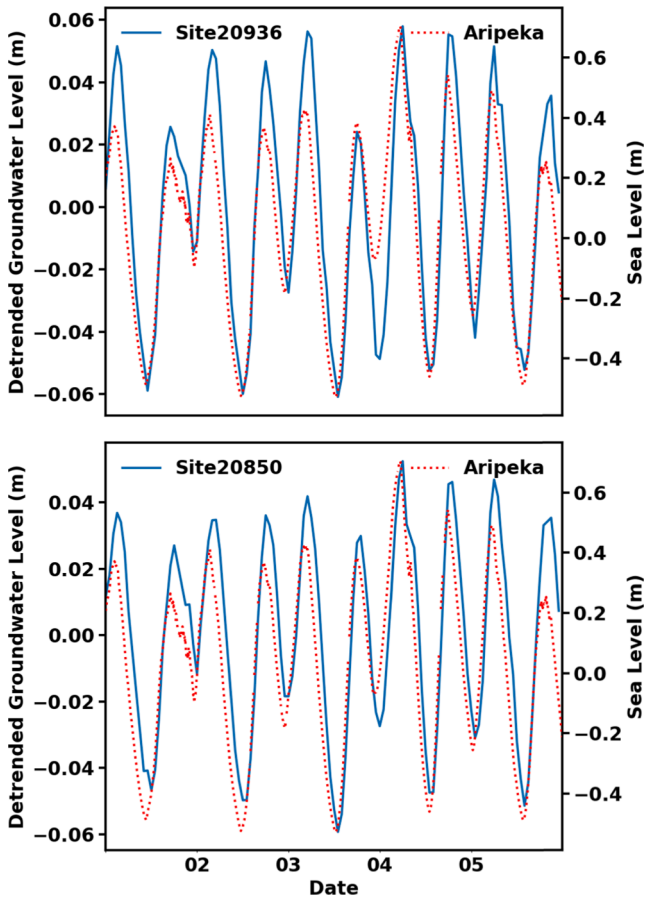

Fig. 6. Comparison between measured sea level and detrended groundwater level from 2019/03/01 to 2019/03/05. top) Aripeka tidal station vs. site 20936 (ROMP TR18-2 Avon Park Formation); and bottom) Aripeka tidal station vs. site 20850 (ROMP TR18-3 Avon Park Formation).

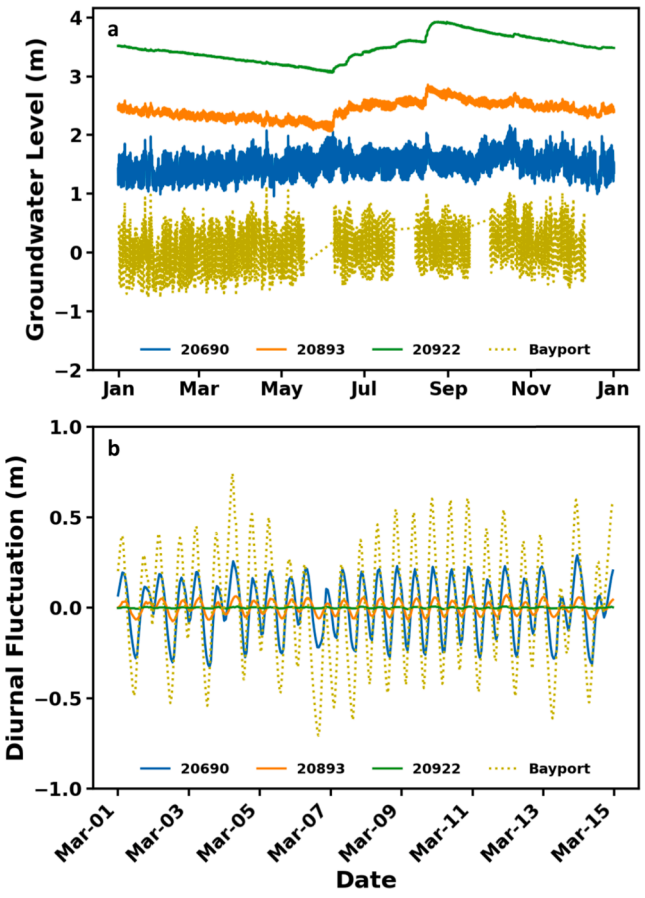

Fig. 7. Measured and detrended groundwater levels in Upper Floridan Aquifer (UFA) along the Weeki Wachee transect. a) Measured groundwater level in year 2019; and b) Detrended groundwater level from 2019/03/01 to 2019/03/15. Yellow dotted lines are measured sea level at Bayport tidal station. Blue line is groundwater level at site 20690 (ROMP TR19-2 Ocala Limestone). Orange line is groundwater level at site 20893 (WW4 Avon Park Formation). Green line is groundwater level at site 20922 (Weeki Wachee Avon Park Formation). (For interpretation of the references to colour in this figure legend, the reader is referred to the web version of this article.)

intervals. Tidal fluctuations using harmonic constants are displayed in Fig. 3 for sea levels. Example of groundwater tidal variation simulated using α_i and ϕ_i is depicted with the fortnight subset for well 20850 in Fig. 4.

In this study, two sets of harmonic constants were computed. As expected, using 4 tidal constituents (M2, S2, O1, and K1) provided a better fitting than 2 tidal constituents (M2 and O1) as exhibited by the higher correlation coefficients in Table 3 than Table 4 for corresponding time series. The surficial aquifer wells (20894, 20848, 20840) failed to yield meaningful values of harmonic constants due to the limited tidal fluctuation. Significant correlation between simulated tidal variation and detrended groundwater level data revealed that the diurnal groundwater variation in Floridan Aquifer wells were impacted by the propagation of ocean tides.

Calculated amplitude (α_i) of two coastal tidal stations were close to each other and the values of tidal phase shift (ϕ_i) show that the tides at Aripeka is about 0.4 h ahead of Bayport. Tides in the area are dominantly semi-diurnal M2 tide ($\alpha_{M2} = 0.31$ m), followed K1 ($\alpha_{K1} = 0.14$ m), S2 ($\alpha_{S2} = 0.14$ m), and O1 ($\alpha_{O1} = 0.14$ m). The harmonic constants computed from observed sea level agrees well with the numerical simulation of He and Weisberg (2002). Computation with 4 tidal constituents (Table 3) or 2 constituents (Table 2) yielded similar values of α_i and ϕ_i for tidal constituents M2 and O1. The same is true for groundwater wells with much smaller fluctuations, reflecting the robustness of the fitting algorithm and further verified that the groundwater variation is indeed caused by ocean tides (Codiga, 2011).

The tidal amplitudes (α_i) estimated from the time series of groundwater levels exhibited the gradual attenuation of tidal fluctuations in

Table 2
Time lagged Pearson correlation coefficient (r_{lag}), relative amplitude (A_R), and time lag (t_{lag}) calculated from cross correlation of detrended groundwater levels at monitoring wells with sea levels measured at corresponding tidal stations (Bayport or Aripeka) in year 2019.

	r_{lag}	A_R	t_{lag}
Site			hour
Weeki Wachee Transect			
20690	0.883	0.38	1.13
20894	0.130	0.0044	3.22
20893	0.863	0.093	1.78
20927	0.613	0.0074	1.58
20922	0.587	0.0073	1.87
Aripeka Transect			
20937	0.498	0.027	1.70
20936	0.840	0.094	0.92
20848	–	–	–
20846	0.854	0.046	1.07
20850	0.888	0.080	0.78
20847	0.817	0.072	0.87
20854	0.679	0.022	3.55
20840	0.036	0.0004	4.43
20841	0.273	0.0031	2.92

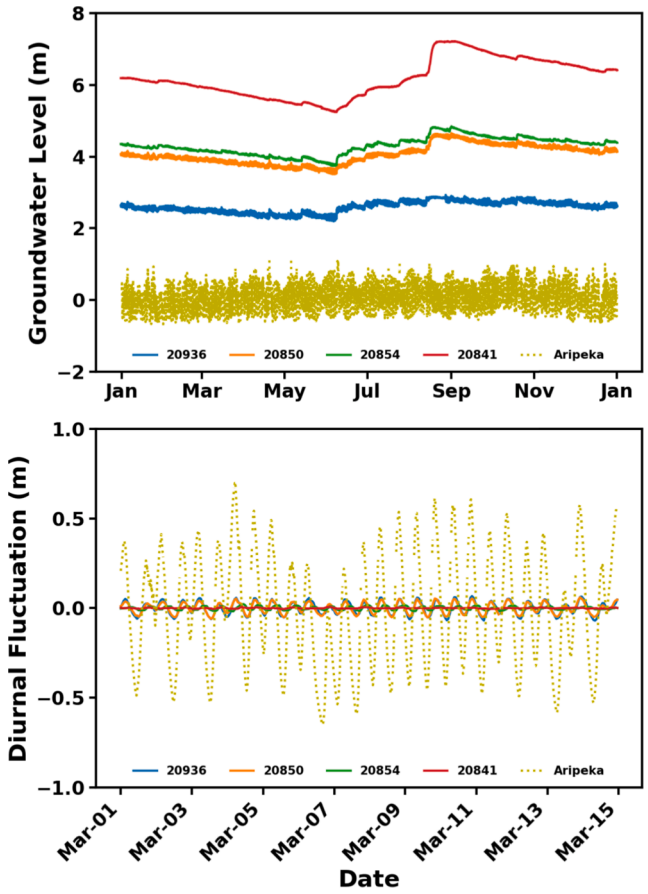

Fig. 8. Measured and detrended groundwater levels in Upper Floridan Aquifer (UFA) along the Aripeka transect. top) Measured groundwater level in year 2019; and bottom) Detrended groundwater level from 2019/03/01 to 2019/03/15. Yellow dotted lines are sea level at Aripeka tidal station.Blue line is groundwater level at site 20936 (ROMP TR18-2 Ocala Limestone). Orange line is groundwater level at site 20850 (ROMP TR18-3 Avon Park Formation). Green line is groundwater level at site 20854 (ROMP TR18-1 Avon Park Formation). Red line is groundwater level at site 20841 (ROMP 97 Avon Park Formation). (For interpretation of the references to colour in this figure legend, the reader is referred to the web version of this article.)

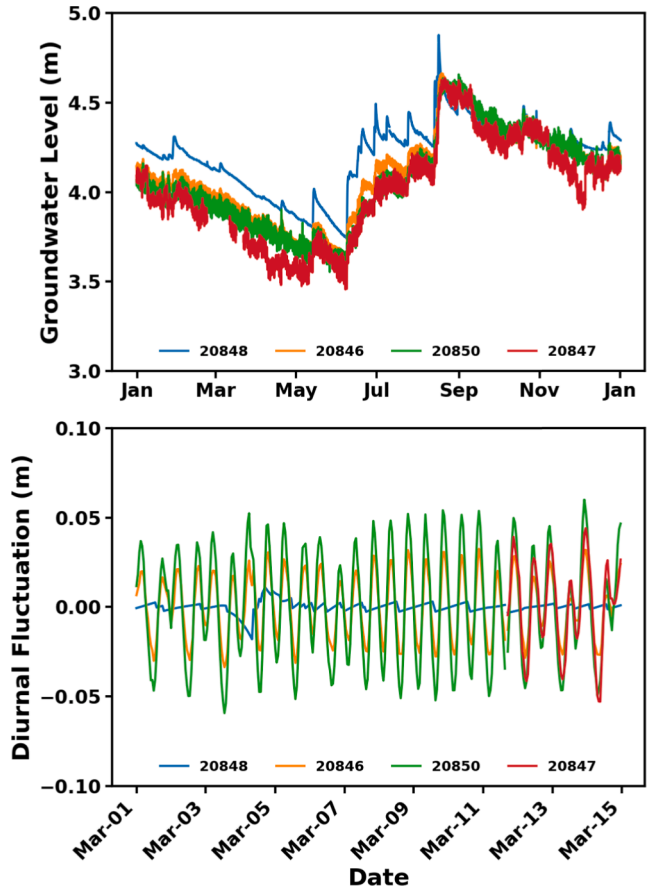

Fig. 9. Measured and detrended groundwater levels at different hydrogeologic layers of monitoring site ROMP TR18-3. top) Measured groundwater level in year 2019; and bottom) Detrended groundwater level from 2019/03/01 to 2019/03/15. Blue line is site 20848 (surficial deposits at 2.1–3.0 m). Orange line is site 20846 (Ocala Limestone at 18–115 m). Green line is site 20850 (Avon Park permeable zone at 146–155 m). Red line is site 20847 (Avon Park Formation at 180–190 m). (For interpretation of the references to colour in this figure legend, the reader is referred to the web version of this article.)

Floridan Aquifer (Tables 3 and 4). The higher values of α_i at wells close to the coast reflected the strong influence of ocean tides on the groundwater elevation. The wells farther inland with diminished α_i demonstrated the damping of tidal waves as it travels through the geological material. The estimated tidal phase shift ϕ_i demonstrated increased time lag of the tidal constituents M2 and O1 with landward distance. But the ϕ_i estimated for tidal constituents K1 and S2 are generally less reliable and the pattern is less clear, which is probably due to the influence of atmospheric pressure (Merritt, 2004). As a result, values of α_i and ϕ_i estimated with M2 and O1 was used for estimating the hydraulic parameters.

3.4. Estimated aquifer diffusivities

The tidal efficiency factor (T_e) and phase lag ($\Delta\phi$) of M2 and O1 tide was computed using the Eqs. (2) and (3) with harmonic constants in Table 4. Specifically, T_e for each of the Floridan Aquifer wells on the Weeki Wachee transect were calculated by dividing their α_i with the α_i of the Bayport coastal station, and α_i of the wells on the Apripeka transect were divided by α_i of the Aripeka station. Similarly, $\Delta\phi$ were calculated from subtracting ϕ_i of wells on the Weeki Wachee transect with ϕ_i of the Bayport station and ϕ_i on the Aripeka transect from ϕ_i of the Aripeka tidal station. The calculated T_e and $\Delta\phi$ are given in Table 5 and plotted as a function of distance to nearest tidal pool in Figs. 10 and 11. Furthermore, T_e and $\Delta\phi$ of wells at site ROMP 18–3 were plotted as a function of casing depth in Fig. 12 to illustrate the vertical variation.

As given in Table 5, the values of tidal efficiency (T_e) of M2 and O1 are close to each other while the $\Delta\phi$ of O1 tide is larger than the M2 tide. Furthermore, the tidal efficiency T_e of both M2 and O1 tide (Table 5) are slightly higher than A_R calculated from cross correlation analysis (Table 2). The phase lag $\Delta\phi$ of M2 tide is close to the corresponding values of t_{lag} in Table 2, while $\Delta\phi$ of O1 tide is generally larger.

Table 6 gives the aquifer diffusivities (D_α or D_ϕ) calculated using either T_e with Eq. (9) or $\Delta\phi$ with Eq. (10) with linear regression of $\ln(T_e)$ or $\Delta\phi$ with the distance to potential discharge location (x). The analysis was conducted separately on the two transects for different hydrogeologic units. On the Weeki Wachee transect, 4 wells (20690, 20893, 20922, and 20927) were used for the Floridan Aquifer, 2 wells (20922 and 20927) for Ocala Limestone and 2 wells (20690 and 20893) for Avon Park Formation. On the Aripeka transect, 7 wells (20937, 20936, 20846, 20850, 20847, 20854, and 20841) were used for Floridan Aquifer, 2 wells (20937and 20846) for Ocala Limestone and 5 wells (20936, 20850, 20847, 20854, and 20841) for Avon Park Formation.

Overall, aquifer diffusivities were higher on the Weeki Wachee transect than that on the Aripeka transect and the Avon Park Formation had higher diffusivities than Ocala Limestone (Table 6). Diffusivity calculated from time lag method (D_ϕ) is 1–6 times higher than D_α

Table 3
Tidal amplitude (α_i) and phase constants (ϕ_i) values (±95% confidence interval) of four major tidal constituents (M2, K1, O1, S2) calculated from measured sea level at tidal stations (Bayport and Aripeka) and detrended groundwater level in monitoring wells in year 2019.

Site		α_i(cm)				ϕ_i(degree)			
	r[a]	M2	K1	O1	S2	M2	K1	O1	S2
Weeki Wachee Transect									
Bayport	0.868	31.1 ± 0.8	14.0 ± 0.7	11.8 ± 0.7	11.0 ± 0.7	313 ± 1	55 ± 3	147 ± 3	231 ± 3
20690	0.927	14.7 ± 0.3	7.9 ± 0.3	6.5 ± 0.4	4.8 ± 0.3	346 ± 1	75 ± 2	166 ± 3	266 ± 3
20894	0.135	0.15 ± 0.03	0.10 ± 0.08	0.07 ± 0.09	0.04 ± 0.03	43 ± 10	122 ± 53	171 ± 70	323 ± 36
20893	0.926	3.81 ± 0.08	1.72 ± 0.09	1.44 ± 0.08	1.4 ± 0.1	3 ± 1	94 ± 4	272 ± 4	186 ± 4
20927	0.655	0.29 ± 0.01	0.18 ± 0.01	0.16 ± 0.03	0.10 ± 0.03	8 ± 3	268 ± 4	97 ± 8	188 ± 14
20922	0.667	0.30 ± 0.01	0.16 ± 0.01	0.15 ± 0.02	0.10 ± 0.03	0 ± 2	262 ± 5	96 ± 8	186 ± 14
Aripeka Transect									
Aripeka	0.856	31.8 ± 0.7	14.7 ± 0.6	12.4 ± 0.6	10.4 ± 0.7	300 ± 1	49 ± 2	141 ± 3	219 ± 4
20937	0.522	1.2 ± 0.1	0.5 ± 0.1	0.3 ± 0.1	0.3 ± 0.1	351 ± 4	73 ± 15	164 ± 18	259 ± 12
20936	0.892	4.0 ± 0.1	1.8 ± 0.1	1.4 ± 0.1	0.9 ± 0.1	328 ± 2	69 ± 4	159 ± 5	222 ± 8
20848	0.058	0.07 ± 0.08	0.01 ± 0.02	0.007 ± 0.02	0.004 ± 0.06	93 ± 76	37 ± 132	78 ± 165	72 ± 202
20846	0.884	1.84 ± 0.04	0.84 ± 0.06	0.73 ± 0.05	0.65 ± 0.06	331 ± 1	69 ± 4	246 ± 3	157 ± 6
20850	0.923	3.21 ± 0.06	1.47 ± 0.08	1.28 ± 0.08	1.14 ± 0.08	323 ± 1	64 ± 3	238 ± 3	154 ± 4
20847	0.887	3.12 ± 0.07	1.46 ± 0.09	1.11 ± 0.09	0.69 ± 0.06	327 ± 1	68 ± 4	156 ± 4	197 ± 6
20854	0.776	0.95 ± 0.03	0.58 ± 0.03	0.40 ± 0.06	0.29 ± 0.05	46 ± 2	289 ± 3	125 ± 7	217 ± 10
20840	0.093	0.03 ± 0.01	0.02 ± 0.01	0.02 ± 0.02	0.02 ± 0.02	281 ± 11	88 ± 21	121 ± 98	285 ± 106
20841	0.367	0.13 ± 0.01	0.12 ± 0.01	0.08 ± 0.03	0.03 ± 0.03	264 ± 4	34 ± 5	137 ± 20	235 ± 62

[a] r: Pearson correlation coefficient between simulated and observed water level.

Table 4
Tidal amplitude (α_i) and phase constants (ϕ_i) values (±95% confidence interval) of major tidal constituents M2 and O1 calculated from measured sea level at tidal stations (Bayport and Aripeka) and detrended groundwater level in monitoring wells in year 2019.

Site		α_i(cm)		ϕ_i(degree)	
	r[a]	M2	O1	M2	O1
Weeki Wachee Transect					
Bayport	0.764	30.9 ± 0.01	11.7 ± 0.02	313 ± 2	147 ± 8
20690	0.789	14.7 ± 0.5	6.6 ± 0.8	346 ± 2	167 ± 7
20894	0.110	0.15 ± 0.03	0.07 ± 0.08	43 ± 10	171 ± 84
20893	0.798	0.038 ± 0.1	0.014 ± 0.3	3 ± 2	186 ± 9
20927	0.503	0.29 ± 0.02	0.09 ± 0.03	9 ± 4	189 ± 25
20922	0.533	0.30 ± 0.02	0.10 ± 0.03	1 ± 4	186 ± 20
Aripeka Transect					
Aripeka	0.752	32.0 ± 0.01	12.6 ± 0.01	301 ± 2	140 ± 7
20937	0.462	1.2 ± 0.1	0.4 ± 0.1	351 ± 4	164 ± 17
20936	0.791	4.0 ± 0.1	1.4 ± 0.2	328 ± 2	159 ± 9
20848	0.058	0.07 ± 0.07	0.01 ± 0.02	93 ± 69	79 ± 157
20846	0.756	1.84 ± 0.06	0.66 ± 0.12	331 ± 2	157 ± 10
20850	0.788	3.2 ± 0.1	1.2 ± 0.2	323 ± 2	154 ± 8
20847	0.783	3.12 ± 0.09	1.1 ± 0.2	327 ± 2	156 ± 9
20854	0.624	0.96 ± 0.05	0.29 ± 0.09	46 ± 4	217 ± 15
20840	0.054	0.02 ± 0.006	0.02 ± 0.020	87 ± 20	284 ± 99
20841	0.225	0.12 ± 0.02	0.03 ± 0.03	34 ± 7	236 ± 83

[a] r: Pearson correlation coefficient between simulated and observed water level.

calculated from the tidal amplitudes. In addition, diffusivities (D_α) calculated using amplitudes of M2 or O1 were close but the D_ϕ calculated from phase lag of M2 was higher than that of O1.

4. Discussion

Observed diurnal variation of groundwater levels in this study reveal that tidal waves can propagate long distances (6–8 km inland) in an unconfined Karst aquifer (Tables 2 and 5). Previous studies suggested that tidal fluctuations were generally damped very quickly as they travel in unconfined aquifer. Observed tidal fluctuation in siliciclastic aquifers often show amplitude ratio less than 1% at distances of tens to hundreds of meters (Nielsen, 1990; Erskine, 1991; Trefry and Johnston, 1998; Mao et al., 2006; Abarca et al., 2013; Shuai et al., 2017; Trglavcnik et al., 2018), which is attributed to the high specific yield of unconfined aquifers (Merritt, 2004). However, tidal waves can travel much further in unconfined karst aquifers due to their large hydraulic conductivity

Table 5
Tidal efficiency (T_e) and phase lag ($\Delta\phi$) in Floridan Aquifer wells calculated from harmonic constants of tidal constituents M2 and O1 given in Table 4 for tidal stations (Bayport and Aripeka) and monitoring wells.

Site	T_e		$\Delta\phi$(hour)	
	M2	O1	M2	O1
Weeki Wachee Transect				
20690	0.48	0.56	1.1	1.4
20893	0.12	0.12	1.7	2.8
20927	0.009	0.008	1.9	3.0
20922	0.010	0.008	1.6	2.8
Aripeka Transect				
20937	0.04	0.03	1.7	1.8
20936	0.13	0.12	0.9	1.4
20846	0.06	0.05	1.1	1.3
20850	0.10	0.09	0.8	1.0
20847	0.10	0.09	0.9	1.2
20854	0.03	0.02	3.6	5.5
20841	0.004	0.002	3.2	6.9

and lower storativity (Rotzoll et al., 2008, 2013). For example, studies of Rotzoll et al. (2008) demonstrate that at 5 km to shore the O1 tide amplitude was 2.7% of the ocean tide and the time lag was around 2 h, which is close to this study (Tables 2 and 5). The strong interaction between seawater and groundwater suggests that coast karst aquifers are especially susceptible to sea level change and saltwater migration (Martin et al., 2012; Perriquet et al., 2014; Xu et al., 2016).

Multi-level observation wells often show that the deeper part of the aquifer has larger tidal amplitude than the shallow layers (Erskine, 1991; Trefry and Johnston, 1998; Ratner-Narovlansky et al., 2020). The increased tidal amplitude with depth was suggested to be a result of the increased confinement and/or decreased storativity (Trefry and Johnston, 1998) and the analytical models developed for the site suggested the leakage effects of the semi-permeable peat layers (Guo et al., 2007). The analytical solution recently developed by Bakker (2019) demonstrates that the tidal signals travel much farther in deeper parts of a multi-layer unconfined aquifer and the effect is enhanced with the presence of thin layers of low permeability, which can partially explain the higher tidal amplitude at the Avon Park formation than the Ocala Limestone at site ROMP TR18-3 (Fig. 12). However, Fig. 12 shows the upper layer of the Avon Park Formation (Well 20850, 146–155 m below ground) has larger tidal amplitude and lower phase lag than the lower Avon Park Formation (Well 20847, 180–190 m below ground). This

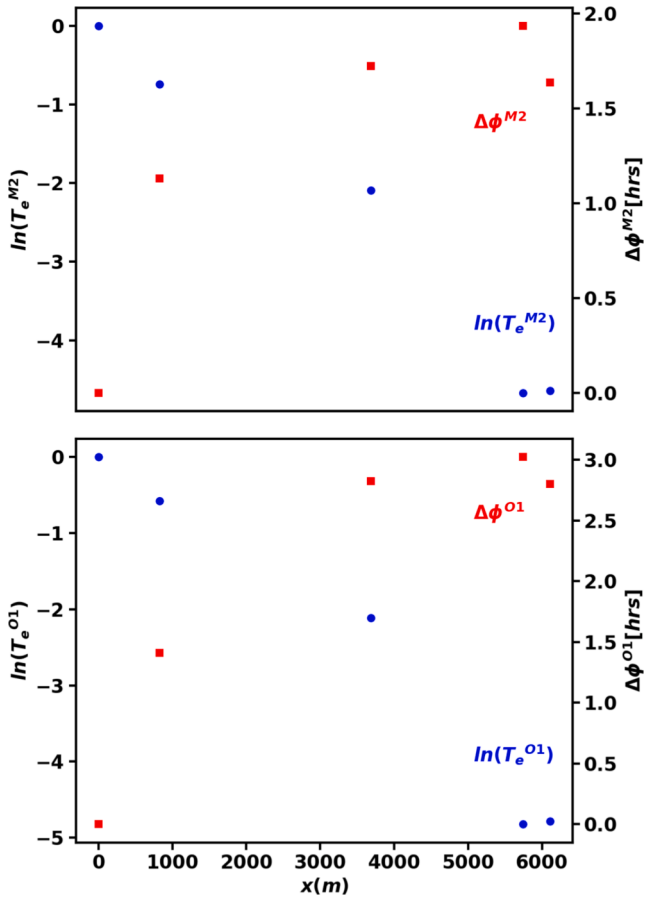

Fig. 10. Tidal efficiency factor (T_e) and phase lag ($\Delta\phi$) as a function of distance to discharge (x) along the Weeki Wachee transect. Top: T_e and $\Delta\phi$ of M2 tide vs. distance; Bottom: T_e and $\Delta\phi$ of O1 tide vs. distance. T_e and $\Delta\phi$ are calculated from harmonic constants of tidal constituents (M2, O1) given in Table 4.

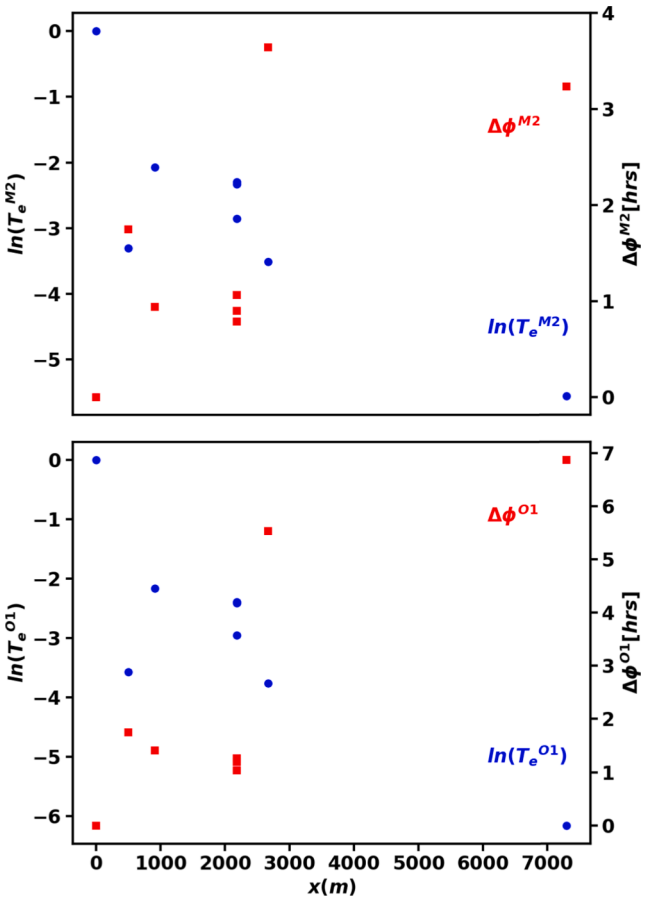

Fig. 11. Tidal efficiency factor (T_e) and phase lag ($\Delta\phi$) as a function of distance to discharge (x) along the Aripeka transect. Top: T_e and $\Delta\phi$ of M2 tide vs. distance; Bottom: T_e and $\Delta\phi$ of O1 tide vs. distance. T_e and $\Delta\phi$ are calculated from harmonic constants of tidal constituents (M2, O1) given in Table 4.

vertical pattern of tidal fluctuation suggests that the tidal wave transmits preferentially in the high permeability zone of the Avon Park Formation and then propagate upward and downward to the layers above and below, which is consistent with the conceptual understanding of the regional hydrogeology (Yobbi, 1992; Knochenmus and Yobbi, 2001).

Application of the Jacob-Ferris equation often assumes a distinctive shoreline as the hydraulic contact with seawater to determine the distance (x) to ocean boundary. However, natural coasts are characterized by complex geomorphology where groundwater discharges into ocean through a range of point, linear, or diffusive features. There are many tidal springs scattered on the coast (Fig. 1) with a direct link to UFA through a complex network of subsurface conduits (Yobbi, 1992; Knochenmus and Yobbi, 2001; Fleury et al., 2007; Menning et al., 2015). In addition, the regional potentiometric surface indicates there is a diffusive upward discharge through vast areas of coastal swamps (Ryder, 1985; Knochenmus and Yobbi, 2001). This composite pattern of hydraulic interaction through rapid flow in fracture networks and slow flow in bulk rock matrices brings a degree of uncertainty in estimation of hydraulic parameter through tidal method (Martin et al., 2012; Perriquet et al., 2014). For example, Martin et al. (2012) applied tidal amplitude method to island karst aquifers and reported that transmissivity of blue holes were 20–60 times higher than that of wells. Further theoretical and numerical modeling is warranted to elucidate the mechanisms of tidal interaction in dual permeability aquifers.

Amplitude based diffusivity (D_α) were consistent for the lunar semi-diurnal (M2) and diurnal (O1) tides, whereas diffusivity derived from time lag (D_ϕ) varied considerably between M2 and O1 tide (Table 6). Assuming linear wave propagation, the Jacob-Ferris equation (Eq. (7)) predicts that semi-diurnal tide dissipated more quickly with less time lag than diurnal tide (Rotzoll et al., 2008). However, in highly heterogenous karst aquifers, turbulent flow in subsurface conduits might be an important or even dominant pathway for the transmission of tidal energies (Martin et al., 2012; Perriquet et al., 2014). Nonlinear wave interaction might arise in such situations and cause the departure from the Jacob-Ferris equation (Xin et al., 2015).

Hydraulic diffusivity estimated from the amplitude-ratio method (D_α) and the time lag method (D_ϕ) demonstrated significant differences (Table 6). Many studies have reported that the Jacob-Ferris equation yields inconsistent diffusivities depending on whether amplitudes or lags are used (Ferris, 1951; Erskine, 1991; Trefry and Johnston, 1998; Trefry and Bekele, 2004; Rotzoll et al., 2008; Trglavcnik et al., 2018) and suggested explanations in terms of depth-dependence of storativities, phreatic influences, or internal layering in hydraulic conductivities, although without conclusive evidence. Trefry and Bekele (2004) defined $\sqrt{D_\alpha/D_\phi}$ as slope factor to measure the departure from the ideal Jacob-Ferris model for tidal wave propagation. Depending on tidal components, hydrogeologic layers, and transects, the slope factor in our study varied between 0.38 and 1.4, which falls in the range of literature values (Trefry and Bekele; 2004). The slope factors for most wells were below unity, which indicated the tidal waves propagate faster than predicted by the analytical equation for 1-D homogeneous groundwater flow. Perriquet et al. (2014) suggested that ratio of D_α/D_ϕ negatively correlates with the contribution of matrix flow relative to conduit flow and classified the hydrodynamic environment into matrix ($D_\phi \gg D_\alpha$), fissure (intermediate D_α/D_ϕ), and conduit ($D_\phi \approx D_\alpha$). Our results in Table 6 indicated that the conduit flow is more prominent in the Avon

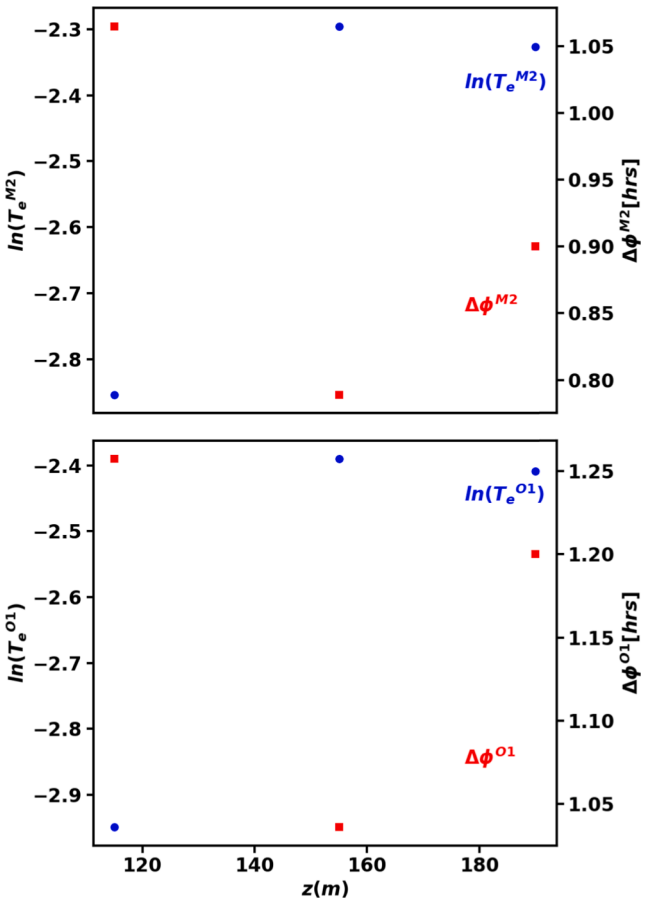

Fig. 12. Tidal efficiency factor (T_e) and phase lag ($\Delta\phi$) as a function of groundwater depth (z) at different hydrogeologic layers of monitoring site ROMP TR18-3. Top: T_e and $\Delta\phi$ of M2 tide vs. casing depth; Bottom: T_e and $\Delta\phi$ of O1 tide vs. casing depth. T_e and $\Delta\phi$ are calculated from harmonic constants of tidal constituents (M2, O1) given in Table 4.

Park Formation than in the Ocala Limestone. In the unconfined UFA, the tidal flow likely first propagates through the dissolved conduits and fractures in high permeable zone of the Avon Park Formation and then expressed in the matrix of hydrogeologic layers above and below. Submarine springs at the ocean end of the conduit networks might be an important interface between seawater and groundwater (Menning et al., 2015; Xu et al., 2016).

Our analysis indicates that dispersivities calculated from the amplitude of dominant tidal component (D_α-M2) provided most robust estimates of the aquifer characteristics of the UFA (1.1×10^7 and 7.1×10^6 m^2 d^{-1} for the Weeki Wachee and Aripeka transects, respectively). Assuming a storativity (S) of 5×10^{-3} based on the range ($5x10^{-4}$ to $5x10^{-2}$) reported for UFA (Southwest Florida Water Management District, 2018), the transmissivity T were calculated as 5.5×10^4 and 3.6×10^4 m^2 d^{-1} for Weeki Wachee and Aripeka transects, respectively. Given a total UFA thickness of 250 m (Fig. 2), the hydraulic conductivity values were estimated as 220 and 143 m/d for Weeki Wachee and Aripeka transects, respectively. Karst aquifers are known for their extremely high heterogeneity and estimation of hydraulic properties is a challenging task due to the complex and dual-porosity flows. In the studied area, reported values of UFA transmissivity from aquifer performance test or slug test ranged 5 orders of magnitude from 21 to 1.5×10^5 m^2 d^{-1}, which is typical of Karst aquifers with extensive conduits (Williams and Kuniansky, 2016). At regional scale, the hydraulic parameters adopted for groundwater flow computation need to combine estimates from pumping test with analysis of potentiometric surface, and further refined through model calibration. Transmissivity values of 4.6×10^4 m^2 d^{-1} for Weeki Wachee and 1.6×10^4 m^2 d^{-1} for Aripeka were used by Knochenmus and Yobbi (2001) in estimation of spring flow and similar values are reported in other Floridan aquifer studies (Ryder, 1985; Williams and Kuniansky, 2016). In this study, the transmissivity estimated from tidal method is remarkably close to that used in regional groundwater flow models (Ryder, 1985; Yobbi, 1992; Knochenmus and Yobbi, 2001; Williams and Kuniansky, 2016). It demonstrated that the tidal method could provide a combined characteristic of the aquifer over a large distance (Trefry and Bekele, 2004). For highly heterogenous karst aquifers, this is especially an advantage over pumping tests which measure aquifer properties at limited distances. The tidal analysis could serve as a valuable tool in developing groundwater models for coastal aquifers.

5. Conclusions

Cross correlation of high frequency fluctuation in groundwater level with tidal level provided insight into the hydrogeologic structures of a multi-layer coastal karst aquifer system. Propagation of tidal signals was observed along the two transects at inland distance up to 7–8 km with a short time lag (1–3 h). The tidal fluctuation in the multi-unit aquifer indicated that the tidal wave preferentially transmitted in the highly permeable zone of the Avon Park formation. Analysis of the hydrogeologic condition suggested there were complex seawater-groundwater interfaces including a preferential pathway through subsurface conduits to coastal springs and a diffusive upward leakage into coastal swamps. Dual permeability transmission appeared to be a significant process linking groundwater levels in karst aquifers with the ocean forces. The Jacob-Ferris equation was successfully employed to quantitatively estimate the aquifer diffusivity and the calculated values were close to that in the regional groundwater flow models. For highly heterogeneous karst aquifers, tidal methods provide a composite description of the hydraulic properties over a long distance, which is more accurate in characterizing regional flow than the pumping-based aquifer test techniques. Further theoretical and numerical investigation of the dual-permeability flow is warranted for the better understanding of the karst aquifer response to ocean forces and more effective management of groundwater resources.

Table 6
Aquifer diffusivity (D_α and D_ϕ) calculated from amplitude (α_i) and phase lag (ϕ_i) of tidal constituents M2 and O1 and slope factor ($\sqrt{D_\alpha/D_\phi}$) for different hydrogeologic units along the Weeki Wachee and Aripeka transects.

Transects	Hydrogeologic Units	M2 Tide			O1 Tide		
		D_α $10^6 m^2 d^{-1}$	D_ϕ $10^6 m^2 d^{-1}$	Slopefactor	D_α $10^6 m^2 d^{-1}$	D_ϕ $10^6 m^2 d^{-1}$	Slopefactor
Weeki Wachee	Floridan Aquifer	11	54	0.45	10	20	0.71
	Ocala Limestone	9.8	67	0.38	9.3	25	0.61
	Avon Park Formation	18	23	0.88	18	9.2	1.40
Aripeka	Floridan Aquifer	7.1	21	0.59	6.1	6.2	0.99
	Ocala Limestone	2.5	15	0.41	2.3	12	0.44
	Avon Park Formation	7.9	21	0.61	6.7	6.0	1.05

Declaration of Competing Interest

The authors declare that they have no known competing financial interests or personal relationships that could have appeared to influence the work reported in this paper.

Acknowledgements

The author thanks Ron Basso, Dr. Xinjian Chen, Robert Peterson, Tamera McBride, Chris Zajac for their constructive discussion and careful review of the manuscript and appreciates the help from Asmita Shukla and Tiffany Carson with data retrieval.

References

Abarca, E., Karam, H., Hemond, H.F., Harvey, C.F., 2013. Transient groundwater dynamics in a coastal aquifer: The effects of tides, the lunar cycle, and the beach profile. Water Resour. Res. 49 (5), 2473–2488. https://doi.org/10.1002/wrcr.20075.

Alcolea, A., Castro, E., Barbieri, M., Carrera, J., Bea, S., 2007. Inverse modeling of coastal aquifers using tidal response and hydraulic tests. Groundwater 45 (6), 711–722.

Ataie-Ashtiani, B., Volker, R.E., Lockington, D.A., 2001. Tidal effects on groundwater dynamics in unconfined aquifers. Hydrol. Process. 15 (4), 655–669.

Bakker, M., 2019. Analytic solutions for tidal propagation in multilayer coastal aquifers. Water Resour. Res. 55 (4), 3452–3464. https://doi.org/10.1029/2019WR024757.

Cartwright, N., Nielsen, P., Li, L., 2004. Experimental observations of watertable waves in an unconfined aquifer with a sloping boundary. Adv. Water Resour. 27 (10), 991–1004.

Codiga, D.L. 2011. Unified Tidal Analysis and Prediction Using the UTide Matlab Functions. Technical Report 2011-01. Graduate School of Oceanography, University of Rhode Island, Narragansett, RI. 59pp. ftp://www.po.gso.uri.edu/ pub/downloads/codiga/pubs/2011Codiga-UTide-Report.pdf.

Chen, X., 2012. Simulating hydrodynamics in a spring-fed estuary using a three-dimensional unstructured Cartesian grid model. Estuarine Coastal Shelf Sci. 115, 246–259.

Erskine, A.D., 1991. The effect of tidal fluctuation on a coastal aquifer in the UK. Groundwater 29 (4), 556–562.

Ferris, J.G., 1951. Cyclic fluctuations of water level as a basis for determining aquifer transmissibility. Int. Assoc. Sci. Hydrol. 148–155 https://doi.org/10.3133/70133368.

Fleury, P., Bakalowicz, M., de Marsily, G., 2007. Submarine springs and coastal karst aquifers: A review. J. Hydrol. 339 (1–2), 79–92.

Guo, Q., Li, H., Boufadel, M.C., Xia, Y., Li, G., 2007. Tide-induced groundwater head fluctuation in coastal multi-layered aquifer systems with a submarine outlet-capping. Adv. Water Resour. 30 (8), 1746–1755. https://doi.org/10.1016/j.advwatres.2007.01.003.

He, R., Weisberg, R.H., 2002. Tides on the west Florida shelf. J. Phys. Oceanogr. 32 (12), 3455–3473.

Jacob, C.E., 1950. Flow of groundwater. In: Rouse, H. (Ed.), Engineering Hydraulics. John Wiley Sons, Hoboken, NY, pp. 321–386.

Jardani, A., Dupont, J.P., Revil, A., Massei, N., Fournier, M., Laignel, B., 2012. Geostatistical inverse modeling of the transmissivity field of a heterogeneous alluvial aquifer under tidal influence. J. Hydrol. 472–473, 287–300.

Jiao, J.J., Tang, Z., 1999. An analytical solution of groundwater response to tidal fluctuation in a leaky confined aquifer. Water Resour. Res. 35 (3), 747–751.

Jiao, J., Post, V. 2019. Coastal Hydrogeology. Cambridge University Press.

Knochenmus, L.A., Yobbi, D.K. 2001. Hydrology of the coastal springs ground-water basin and adjacent parts of Pasco, Hernando, and Citrus Counties, Florida. Water-Resources Investigations Report 2001-4230. Tallahassee, Florida.

Kong, J., Xin, P., Hua, G.-F., Luo, Z.-Y., Shen, C.-J., Chen, D., Li, L., 2015. Effects of vadose zone on groundwater table fluctuations in unconfined aquifers. J. Hydrol. 528, 397–407.

Kuan, W.K., Jin, G., Xin, P., Robinson, C., Gibbes, B., Li, L., 2012. Tidal influence on seawater intrusion in unconfined coastal aquifers. Water Resour. Res. 48, W02502. https://doi.org/10.1029/2011WR010678.

Li, H., Jiao, J.J., 2001. Tide-induced groundwater fluctuation in a coastal leaky confined aquifer system extending under the sea. Water Resour. Res. 37 (5), 1165–1171.

Li, H., Boufadel, M.C., Weaver, J.W., 2008. Tide-induced seawater–groundwater circulation in shallow beach aquifers. J. Hydrol. 352 (1–2), 211–224.

Maas, C., De Lange, W.J., 1987. On the negative phase shift of groundwater tides near shallow tidal rivers—The Gouderak anomaly. J. Hydrol. 92 (3-4), 333–349.

Mao, X., Enot, P., Barry, D.A., Li, L., Binley, A., Jeng, D.-S., 2006. Tidal influence on behaviour of a coastal aquifer adjacent to a low-relief estuary. J. Hydrol. 327 (1–2), 110–127.

Martin, J.B., Gulley, J., Spellman, P., 2012. Tidal pumping of water between Bahamian blue holes, aquifers, and the ocean. J. Hydrol. 416-417, 28–38.

Menning, D.M., Wynn, J.G., Garey, J.R., 2015. Karst estuaries are governed by interactions between inland hydrological conditions and sea level. J. Hydrol. 527, 718–733.

Merritt, M.L. 2004. Estimating Hydraulic Properties of the Floridan Aquifer System by Analysis of Earth-Tide, Ocean-Tide, and Barometric Effects, Collier and Hendry Counties, Florida. U.S. Geological Survey Water-Resources Investigations Report 03-4267. Tallahassee, Florida.

Mulligan, A.E., Langevin, C., Post, V.E. 2011. Tidal boundary conditions in SEAWAT. Groundwater, 49(6), 866–879.

Nielsen, P., 1990. Tidal dynamics of the water table in beaches. Water Resour. Res. 26 (9), 2127–2134.

Perriquet, M., Leonardi, V., Henry, T., Jourde, H., 2014. Saltwater wedge variation in a non-anthropogenic coastal karst aquifer influenced by a strong tidal range (Burren, Ireland). J. Hydrol. 519, 2350–2365.

Pauw, P.S., Oude Essink, G.H.P., Leijnse, A., Vandenbohede, A., Groen, J., van der Zee, S. E.A.T.M., 2014. Regional scale impact of tidal forcing on groundwater flow in unconfined coastal aquifers. J. Hydrol. 517, 269–283.

Post, V.E.A., 2011. A new package for simulating periodic boundary conditions in MODFLOW and SEAWAT. Comput. Geosci. 37 (11), 1843–1849. https://doi.org/10.1016/j.cageo.2011.01.012.

Ratner-Narovlansky, Y., Weinstein, Y., Yechieli, Y., 2020. Tidal fluctuations in a multi-unit coastal aquifer. J. Hydrol. 580, 124222. https://doi.org/10.1016/j.jhydrol.2019.124222.

Riedel, T., Lettmann, K., Beck, M., Brumsack, H.-J., 2010. Tidal variations in groundwater storage and associated discharge from an intertidal coastal aquifer. J. Geophys. Res. 115, C04013. https://doi.org/10.1029/2009JC005544.

Rotzoll, K., El-Kadi, A.I., Gingerich, S.B., 2008. Analysis of an unconfined aquifer subject to asynchronous dual-tide propagation. Groundwater 46 (2), 239–250.

Rotzoll, K., Gingerich, S.B., Jenson, J.W., El-Kadi, A.I., 2013. Estimating hydraulic properties from tidal attenuation in the Northern Guam Lens Aquifer, territory of Guam, USA. Hydrogeol. J. 21 (3), 643–654.

Ryder, P.D. 1985. Hydrology of the Floridan Aquifer System in West-Central Florida. U.S. Geological Survey Professional Paper 1403-F. Washington, DC.

Schaff, D.P., Richards, P.G., 2014. Improvements in magnitude precision, using the statistics of relative amplitudes measured by cross correlation. Geophys. J. Int. 197 (1), 335–350.

Shuai, P., Knappett, P.S.K., Hossain, S., Hosain, A., Rhodes, K., Ahmed, K.M., Cardenas, M.B., 2017. The impact of the degree of aquifer confinement and anisotropy on tidal pulse propagation. Groundwater 55 (4), 519–531.

Southwest Florida Water Management District, 2018. Aquifer Characteristics within the Southwest Florida Water Management District. Brooksville, Florida. https://www.swfwmd.state.fl.us/sites/default/files/medias/documents/Aquifer%20Characteristics%20Document%207-2018.pdf.

Sun, P., Li, H., Boufadel, M.C., Geng, X., Chen, S., 2008. An analytical solution and case study of groundwater head response to dual tide in an island leaky confined aquifer. Water Resour. Res. 44 (12) https://doi.org/10.1029/2008WR006893.

Trefry, M.G., Johnston, C.D., 1998. Pumping test analysis for a tidally forced aquifer. Groundwater 36 (3), 427–433.

Trefry, M.G., Bekele, E., 2004. Structural characterization of an island aquifer via tidal methods. Water Resour. Res. 40, W01505. https://doi.org/10.1029/2003WR002003.

Trefry, M.G., McLaughlin, D., Lester, D.R., Metcalfe, G., Johnston, C.D., Ord, A., 2011. Stochastic relationships for periodic responses in randomly heterogeneous aquifers. Water Resour. Res. 47, W08527. https://doi.org/10.1029/2011WR010444.

Trglavcnik, V., Morrow, D., Weber, K.P., Li, L., Robinson, C.E., 2018. Analysis of tide and offshore storm-induced water table fluctuations for structural characterization of a coastal island aquifer. Water Resour. Res. 54 (4), 2749–2767. https://doi.org/10.1002/wrcr.v54.410.1002/2017WR020975.

Van der Kamp, G. 1972. Tidal fluctuations in a confined aquifer extending under the sea: International Geological Congress, 24(11), 101–106.

Williams, L.J., Kuniansky, E.L. 2016. Revised hydrogeologic framework of the Floridan aquifer system in Florida and parts of Georgia, Alabama, and South Carolina (ver 1.1, March 2016): U.S. Geological Survey Professional Paper 1807, 140 p., 23 pls, https://doi.org/10.3133/pp1807.

Xia, Y., Li, H., Boufadel, M.C., Guo, Q., Li, G., 2007. Tidal wave propagation in a coastal aquifer: Effects of leakages through its submarine outlet-capping and offshore roof. J. Hydrol. 337 (3–4), 249–257.

Xin, P., Wang, S.S.J., Lu, C., Robinson, C., Li, L., 2015. Nonlinear interactions of waves and tides in a subterranean estuary. Geophys. Res. Lett. 42 (7), 2277–2284. https://doi.org/10.1002/2015GL063643.

Xu, Z., Bassett, S.W., Hu, B., Dyer, S.B., 2016. Long distance seawater intrusion through a karst conduit network in the Woodville Karst Plain, Florida. Sci. Rep. 6 (1), 1–10.

Yobbi, D.K. 1992. Effects of Tidal Stage and Ground-Water Levels on the Discharge and Water Quality of Springs in Coastal Citrus and Hernando Counties, Florida. U.S. Geological Survey Water-Resources Investigations Report 92-4069. Tallahassee, Florida.